Catalysis Today 213 (2013) 81–86

Contents lists available at SciVerse ScienceDirect

Catalysis Today

journal homepage: www.elsevier.com/locate/cattod

Influence of Ge content on the activity of Ru–Ge–B/Al_2O_3 catalysts for selective hydrogenation of methyl oleate to oleyl alcohol

María A. Sánchez [a], Vanina A. Mazzieri [a], Marcelo Oportus [b], Patricio Reyes [b], Carlos L. Pieck [a,*]

[a] Instituto de Investigaciones en Catálisis y Petroquímica (INCAPE) (FIQ-UNL, CONICET), Santiago del Estero 2654, S3000AOJ Santa Fe, Argentina
[b] Departamento de Físico Química, Facultad de Ciencias Químicas, Universidad de Concepción, Casilla 160-C, Concepción, Chile

ARTICLE INFO

Article history:
Received 17 December 2012
Received in revised form 19 February 2013
Accepted 20 February 2013
Available online 20 April 2013

Keywords:
Selective hydrogenation
Methyl oleate
Oleyl alcohol
Ru–Ge–B/Al_2O_3

ABSTRACT

The influence of Ge content on the activity and selectivity of Ru–Ge–B/Al_2O_3 catalysts for the hydrogenation of methyl oleate to oleyl alcohol was studied. The results of catalyst characterization by TPR and XPS show that Ge is deposited on both the metal function aggregates and on the support surface. The fraction of Ge deposited on the metal function is in strong interaction with Ru, so that its metallic activity is significantly modified. Both dehydrogenating and hydrogenolytic activities of Ru are strongly diminished by Ge addition. The Ge/Ru = 2 is the optimum ratio for oleyl alcohol production.

1. Introduction

The hydrogenolysis of methyl esters of fatty acids to produce fatty alcohols is an important step in the production of detergents from natural raw materials. Unsaturated fatty alcohols, in particular, are used in industry for the manufacture of liquid detergents, cosmetics, pharmaceuticals and defoamers. These alcohols are generally obtained in laboratory scale from the hydrogenation of carbonyl compounds with classical reducing agents such as alkaline hydrides ($LiAlH_4$, $NaBH_4$). Industrial production of fatty alcohols is currently done using a catalytic hydrogenation technology with fatty acids or its methyl esters as raw materials and copper chromite [1] or zinc chromite [2–5] as catalysts. Unfortunately, the intrinsic low activity of such catalysts requires the operation at severe conditions (250–300 °C; 20–35 MPa) [6] which favor the non selective hydrogenation of C—C bonds which is undesirable instead the required hydrogenation of carbonyl or carboxymethyl groups. Metallic Cu^0 has a lower intrinsic hydrogenating activity, has poor resistance to thermal sintering and weak mechanical stability. Some promoters like Cr are usually added to improve its physicochemical and textural properties [7]. The use of promoters can also improve the hydrogenating activity so less severe operating conditions are required.

There is currently great interest in alternative, noble metal based catalysts more selective toward the hydrogenation of carbonyl or carboxymethyl groups without affecting the olefinic bonds present in the original fatty molecule. Those catalysts should also be more active so less severe operating conditions could be used. The rate of hydrogenation of olefinic bonds with group VIII (Pt, Rh, Ru, etc.) catalysts is normally higher than for C—O bonds hydrogenation [6]. For example, Ru–Sn and Rh–Sn catalysts supported on Al_2O_3, SiO_2, or ZrO_2 for the hydrogenation of methyl laurate or methyl palmitate have been tried [8]. In the case of the hydrogenation of methyl oleate over Ru–Sn/TiO_2 catalysts it has been found [9] that Sn addition decreases the overall conversion but greatly improves the yield to alcohols, particularly the unsaturated ones. Some works on these novel catalysts have shown that Ru–Sn–B supported catalysts [10,11] can be active and selective for the production of unsaturated fatty alcohols from the corresponding fatty acid methyl esters [6–13]. It was found for example that methyl oleate can be selectively hydrogenated to oleyl alcohol using a Ru–Sn–B/Al_2O_3 catalyst at 4.5 MPa and 270 °C. Good activity (80% conversion) and selectivity (80%) levels were observed with a catalyst prepared impregnating the support with $RuCl_3$ and $SnCl_2$ (Sn/Ru = 2) and then reducing these deposited salts with sodium borohydride [14,15]. The better performance of noble metal supported catalysts promoted with Sn, Ge or Fe is currently explained by an activation of carbonyl double bonds through an interaction of its free electronic pair with the promoter atoms [16]. As the promoter/Ru ratio increases, there are fewer Ru atoms exposed

* Corresponding author. Tel.: +54 342 4533858; fax: +54 342 4531068.
E-mail address: pieck@fiq.unl.edu.ar (C.L. Pieck).

0920-5861/$ – see front matter © 2013 Elsevier B.V. All rights reserved.
http://dx.doi.org/10.1016/j.cattod.2013.02.028

on the catalyst surface so the promoter has a physical poisoning effect (blocking of surface Ru atoms). Besides, the possible formation of Ru/promoter alloys could also strongly affect the catalytic properties of the metallic phase [17]. Echeverri et al. [14] have reported that the selectivity to the unsaturated alcohol is higher for the bimetallic catalysts prepared from chlorine-free precursors. Surface chlorine would prevent an effective interaction between ruthenium and tin species.

Other researchers have reported the selective hydrogenation of citral to unsaturated alcohols using Pt/Ti–Al_2O_3 catalysts promoted by Ge [18]. They found that Ge addition greatly improves the selectivity to the unsaturated alcohols.

The selective hydrogenation of methyl oleate to obtain oleyl alcohol using Ru/Al_2O_3 catalysts modified by the incorporation of Ge and B is studied in this work to complete a series of previous works on the modification of supported Ru catalysts by incorporation of modifiers and promoters.

2. Experimental

2.1. Catalysts preparation

The support used was a commercial high-purity γ-alumina (Cyanamid Ketjen CK 300). Main impurities were Na (5 ppm), Fe (150 ppm) and S (50 ppm). The extruded alumina pellets were ground and sieved and the 35–80 mesh fraction was separated and calcined under flowing air (3 h at 650 °C). The specific surface area of this support was 180 $m^2\,g^{-1}$, the pore volume 0.49 $cm^3\,g^{-1}$ and the average pore radius 5.4 nm. The catalysts were prepared by the incipient wetness method: this procedure was described by Shoenmaker-Stolk et al. [19]. The support was wetted with exactly the pore volume of an aqueous solution of metal precursor salts in the required amounts to achieve the desired metal content. Wetted samples were left to stand during 12 h. A step of reduction with excess sodium borohydryde aqueous solution was then performed. Then the solids were filtered, washed with water until acid neutrality and dried during 4 h at 120 °C under flowing N_2. The last preparation step included reduction with H_2 at 300 °C, cooling, and hydrogen purging with N_2 as described before. The amount and concentration of the solutions were adjusted in order to have a 1.0 wt% of Ru on the final catalyst whereas the Ge content was varied in the range 0.5–4.0 wt%. As all the catalysts are supported onto Al_2O_3 they will named only by the metallic compound, i.e., Ru(1.0)–Ge(0.5)–B, being the number between parentheses the corresponding metal weight percentages.

2.2. Catalysts characterization

2.2.1. Evaluation of the Ru, Ge and B contents

The composition of the metallic phase was determined by inductively coupled plasma-optical emission spectroscopy (ICP-OES, Perkin Elmer, Optima 2100 DV) after digestion in an acid solution and dilution.

2.2.2. Temperature programmed reduction

TPR tests were performed in an Ohkura TP2002 apparatus equipped with a thermal conductivity detector. Prior to reduction, the calcined catalysts (ca. 0.1 g loaded in a U-shaped reactor) were heated at 120 °C and kept at that temperature for 1 h in a stream of argon to remove water. The samples were then cooled to room temperature under this atmosphere and switched to 5% H_2/Ar (50 ml min^{-1}) mixture. Then it was heated from room temperature to 850 °C at a heating rate of 10 °C min^{-1}. The effluent gas was passed through a cold trap before TCD cell in order to remove water from the exit stream.

2.2.3. Cyclohexane dehydrogenation

The dehydrogenation of cyclohexane (CH) to benzene is a reaction that is insensitive to the structure of the metallic active site and was used as one of the test reactions for the metallic function. It was performed under the following conditions: catalyst mass = 0.1 g, T = 300 °C, P = 1 atm, hydrogen flow = 80 $cm^3\,min^{-1}$, cyclohexane flow = 1.61 $cm^3\,h^{-1}$ (Merck 99.9%). The catalyst sample was previously reduced at 500 °C under flowing H_2 during 1 h. Cyclohexane was supplied by Merck (spectroscopy grade, 99.9% pure), with a specified sulphur upper limit of 0.001%.

2.2.4. CO chemisorption

The experiments were performed in a chemisorption equipment designed ad-hoc. The reduced catalyst was placed in a quartz reactor and reduced further in situ under a hydrogen stream (500 °C, 1 h, 60 $cm^3\,min^{-1}$). Then, the carrier was switched to N_2 and the adsorbed hydrogen was desorbed (500 °C, 60 $cm^3\,min^{-1}$) for 1 h; then the cell was cooled down to room temperature. Then 0.25 cm^3 pulses of diluted CO (3.5% CO in N_2) were fed to the reactor. Non chemisorbed CO was quantitatively transformed into CH_4 over a Ni/Kieselgur catalyst and detected in a flame ionization detector connected on-line.

2.2.5. X-ray photoelectron spectroscopy (XPS)

The XPS measurements were carried out using a multitechnique system (SPECS) equipped with a dual Mg/Al X-ray source and a hemispherical PHOIBOS 150 analyzer operating in the fixed analyzer transmission (FAT) mode. The spectra were obtained with pass energy of 30 eV; an Mg Ka X-ray source was operated at 200 W and 12 kV. The working pressure in the analyzing chamber was less than 5.9×10^{-7} Pa. The XPS analyses were performed on the solids after treatment with hydrogen/Argon at 300 °C carried out in the reaction chamber of the spectrometer. The spectral regions corresponding to Ru $3d_{5/2}$ and Ge $3d_{5/2}$ core levels were recorded for each sample. The calibration of the spectra was performed with the Al 2p line (74.4 eV) from an Al_2O_3 support. The data treatment was performed with the Casa XPS program (Casa Software Ltd., UK). The peak areas were determined by integration employing a Shirley-type background. Peaks were considered to be a mixture of Gaussian and Lorentzian functions in a 70/30 ratio. For the quantification of the elements, sensitivity factors provided by the manufacturer were used.

2.2.6. Transmission electron microscopy

Transmission electron micrographs (TEM) and electron diffraction patterns (ED) were obtained in a Jeol JEM 1200 EXII microscope. The supported catalysts were ground in an Agatha mortar and dispersed in ethanol. A diluted drop of each dispersion was placed on a 150 mesh copper grid coated with carbon.

2.2.7. Methyl oleate hydrogenation

A stainless steel stirred autoclave (240 cm^3 effective volume) was used for these reaction tests. Operating conditions were: temperature: 290 °C; hydrogen pressure: 50 atm; mass of catalyst: 1 g; reactant (methyl oleate, 99% from Sigma–Aldrich) volume: 4 cm^3; solvent (*n*-dodecane) volume: 60 cm^3 and stirring speed: 800 rpm. Reactant and solvent (methyl oleate and *n*-dodecane) were Sigma–Aldrich 99% grade.

Reaction products were analyzed by GC (Varian 3400 CV) using a Chevron ZB-FFAP capillary column (length: 30 m, inner diameter: 0.25 mm ID). Analysis conditions were: injector temperature: 220 °C, column temperature: 200 °C for 1 min, 2 °C min^{-1} ramp up to 260 °C and then isothermal. Identification of reaction products was previously done by GC–MS (Shimadzu QP-50000), using the same capillary column. Only oleyl alcohol, methyl stearate, stearyl

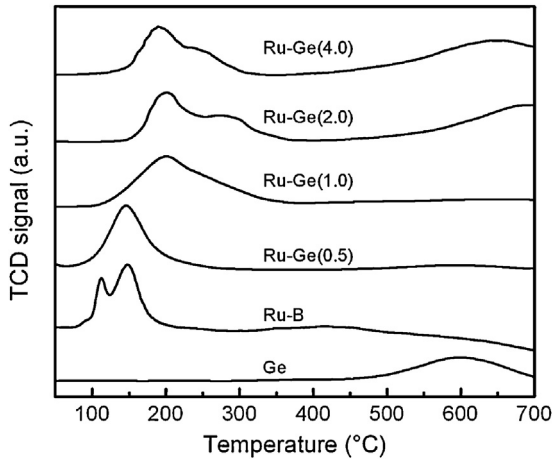

Fig. 1. TPR of Ru(1%)–Ge(x)–B/Al_2O_3 catalysts.

alcohol and methyl oleate were only detected as significantly compounds in the reactor samples.

3. Results and discussion

Chemical analysis determined by inductively coupled plasma-optical emission spectroscopy of catalysts shows metal contents in close agreement with the expected theoretical ones for all the samples. The specific surface area of the support (180 $m^2\,g^{-1}$) does not change after metal precursors impregnation due to the small quantities added.

Temperature programmed reduction profiles of bimetallic and monometallic catalysts are shown in Fig. 1. The monometallic Ge catalyst displays a reduction peak at ca. 600 °C which can be attributed to the reduction of Ge oxide species [20]. On the other hand, it can be seen that the monometallic Ru catalyst has two reduction peaks at 120 °C and 173 °C. Previous studies [6] indicate that the first peak may be due to the reduction of chlorinated Ru species. The second, smaller peaks could be assigned to ruthenium oxide reduction [21,22]. All bimetallic catalysts have a reduction peak located near 200 °C which is currently assigned to the reduction of RuO_2 to Ru° [23]. At higher Ge loadings the reduction of Ru oxide species proceeds at higher temperatures and the intensity of the reduction peak corresponding to segregated Ge species (600 °C) increases. The Ru–Ge(x)–B catalysts with lower content of Ge (i.e. $x \leq 1$) do not show reduction peaks at higher temperatures indicating that all the Ge is reduced a lower temperature. The shift of the reduction peak of Ru oxide species was previously found for the Pt–Ge/Al_2O_3 catalysts. It was attributed to a hindering of the reduction of Pt species by a stronger interaction with Ge or to physical blocking [24]. The temperature range of reduction between 200 °C and 350 °C can be assigned to Ge species in strong interaction with Ru.

The metallic accessibility obtained by CO chemisorption and the mean cyclohexane conversion are reported in Table 1 for the Ru(1%)–Ge(x)–B catalysts. It can be seen that Ge addition decreases

Table 1
Metal dispersion (%), metal particle size (nm) and cyclohexane conversion of the Ru–Ge(x)–B/Al_2O_3 catalysts.

Catalysts	CO/Ru	d_{TEM} (nm)	CH conversion (%)
Ru–B	58	2.0	43.2
Ru–Ge(0.5)–B	26	–	28.1
Ru–Ge(1.0)–B	6	5.3	11.8
Ru–Ge(2.0)–B	2	6.3	5.0
Ru–Ge(4.0)–B	–	–	4.8

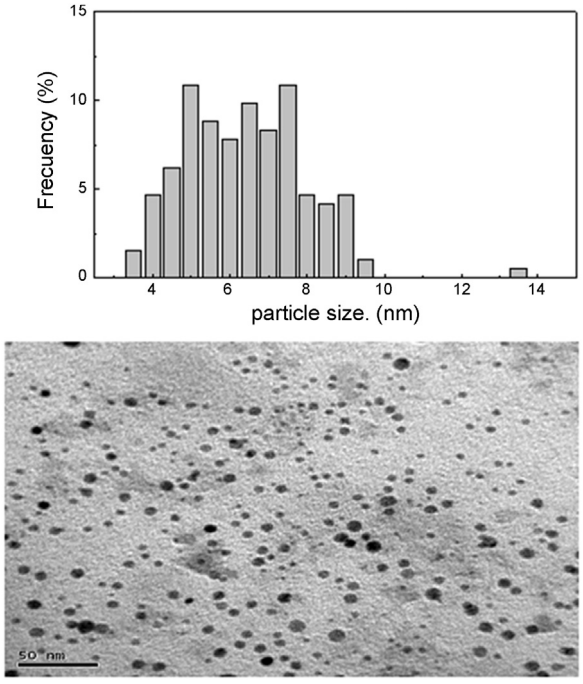

Fig. 2. TEM and particle size distribution of the RRu–Ge(1.0)–B/Al_2O_3h–Ge(1.0)–B/Al_2O_3 catalyst.

both the CO chemisorption as well as the activity for dehydrogenation of cyclohexane. This phenomenon is easily explained taking into account that Ge could not chemisorbed CO and they have not dehydrogenation activity. Thus, by a geometric effect the Ge species block the actives sites of Ru. These results are in agreement with TPR studies where the reduction profiles show a strong interaction between Ru and Ge.

Fig. 2 shows a representative TEM micrograph and metal particle size distribution of the studied catalysts, and the results are also compiled in Table 1. Ru particle size in the monometallic catalysts displays an average of 2.0 nm with a narrow size distribution. An increase in the particle size and a broadening in the particle size distribution take place in the bimetallic catalysts. This may be attributed to the fact that Ge is partially located close to Ru species in agreement with chemisorption TEM and hydrogenation results.

XPS study is carried out for the chemical states identification of elements present in the Ru–Ge–B catalyst system. XPS spectra for bimetallic catalysts are given in Fig. 3. As the peak of Ru $3d_{3/2}$ overlaps with that of C 1s, the peak of Ru $3d_{5/2}$ was employed for all the catalysts to determine the chemical state of Ru. XPS results show that Ru° metallic species are present in all catalysts with binding energy (BE) values in the range between 279.2 eV and 280.1 eV, in accordance with the values for metallic Ru reported in the literature [15,17,25]. An additional $3d_{5/2}$ peak about 284 eV was also found which can be assigned to the presence of oxidated Ru species. Similar results were reported by Elmasides et al. [26] who found that after a higher reduction temperature (550 °C), about 20% of the Ru remains in the Ru^{2+} state on Al_2O_3. An incomplete reduction of Ru has previously been reported for monometallic Ru/Al_2O_3 catalysts [27].

A single peak of B 1s (not shown) found at 192.8 eV in Ru–Ge–B catalyst can be attributed to B^{3+}, possibly in the form of sodium borate adsorbed on the alumina support near to the Ru clusters. In the B 1s spectrum, no peak around 187 eV was observed, indicating the absence of metal boride in the present catalyst system [28]. The −0.5 eV shift observed in the bond energy of B^{3+} implies an increase in its electronic density possibly due to a charge transfer from Ru atoms.

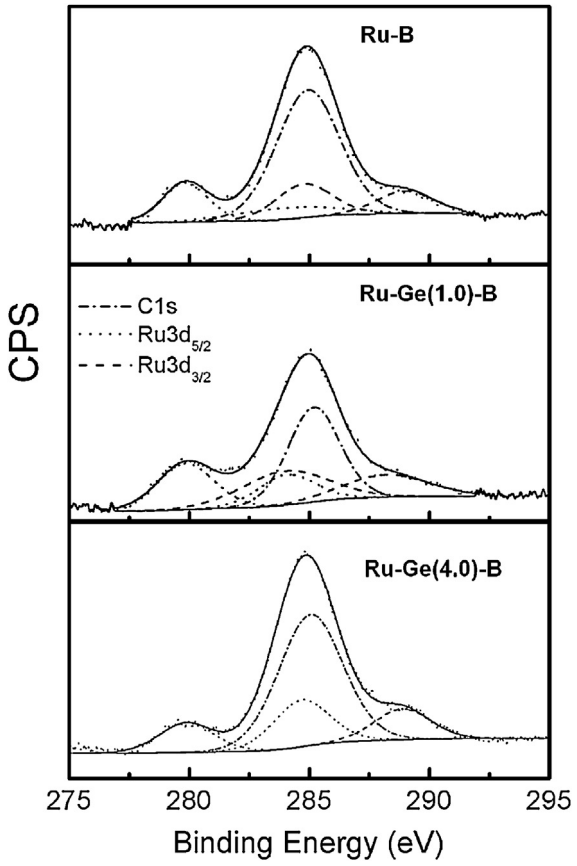

Fig. 3. XPS signals of Ru $3d_{5/2}$ in the Ru–Ge(x)–B/Al_2O_3 catalysts.

The Ge $3d_{5/2}$ peak was used to determinate the oxidation state of Ge and its superficial concentration. This peak can be deconvoluted in two peaks associated to Ge° (29.8 eV) and Ge^{n+} (32.2 eV) (results not shown). It is noted that these oxidized Ge species cannot be discriminated into Ge^{2+} or Ge^{4+} since the binding energy of both Ge oxides are very close [29]. However, from XPS results it was possible to evaluate the percentage of the Ge reduced and the oxidized species, resulting $Ge^{\circ}/(Ge^{n+} + Ge^{\circ}) = 1.00$ and 0.78 for Ru–Ge(1.0)–B and Ru–Ge(4.0)–B catalysts, respectively. This clearly shows that as the Ge content increases lower amount of Ge is reduced to metallic state. The presence of Ge° can be explained by the catalytic effect of Ru on the reduction of Ge oxides because by TPR it was determined that Ge begin the reduction at 500 °C while the reduction pretreatment performed before XPS analysis was carried out at 300 °C.

Ru/Al, Ge/Al, and $Ru^{\circ}/(Ru^{\circ} + Ru^{n+})$ surface atomic ratios as calculated from XPS data and Ru/Al and Ge/Al bulk from chemical analysis are displayed in Table 2. According to the chemical (bulk) composition and XPS analysis of catalysts the Ru/Al atomic ratios from XPS data are higher than those obtained from chemical analysis. Therefore there are Ru surface enrichment for all Ru–Ge catalysts. Concerning the Ge/Al atomic ratio, it can be also observed Ge surface enrichment. A surface enrichment of Ru species was previously found by Pouilloux et al. [15].

It must be pointed out that the B-containing catalyst exhibited a higher proportion of reduced Ru that the catalyst prepared without B ($Ru^{\circ}/(Ru^{\circ} + Ru^{n+}) = 0.32$). It can be seen in Table 2 that the increases of Ge decreases the $Ru^{\circ}/(Ru^{\circ} + Ru^{n+})$ ratio in agreement with TPR results where it was reported a shift of reduction peak of Ru oxides species at higher temperatures.

The results show the existence of an important amount of Ge° that could be alloyed with Ru, together with an important fraction of oxidized Ge, likely placed both in the metallic phase and on the support. These conclusions confirm the results obtained from cyclohexane dehydrogenation, CO chemisorption and TPR. Ru–Ge–B catalysts would show an important fraction of intermetallic alloys or a strong interaction between the metals but a poor hydrogenation catalytic performance. These last results are in agreement with those reported in the literature for the Pt–Ge/Al_2O_3 catalysts. Borgna et al. [30] found that the Ge addition to Pt in catalysts supported on γ-Al_2O_3 produces an enhancement of the electrophilic character of Pt and it also geometrically modifies the surface Pt with the consequent drops of the dehydrogenation activity. de Miguel et al. [20] reported that in Pt–Ge/γ-Al_2O_3 catalysts, small amounts of free Pt would exist and the alloyed phase would be important, a certain blocking of Pt by Ge atoms being also found.

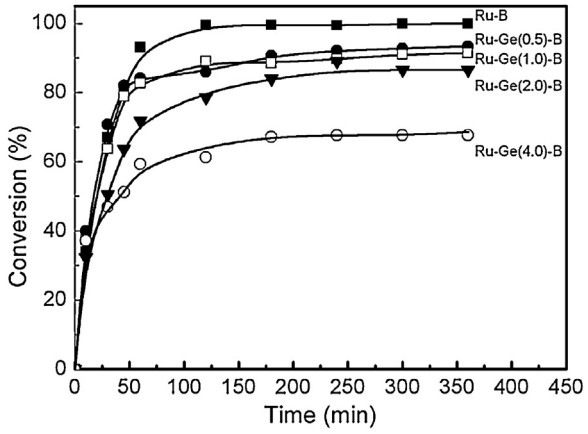

Fig. 4. Hydrogenation of methyl oleate on the Ru(1%)–Ge(x)–B/Al_2O_3 catalysts.

Fig. 4 shows the conversion values of methyl oleate as a function of time for the studied catalysts. The conversion values at the end of experiments (360 min) follow the order reported in Table 1, as it is expected. Similar tendencies were found on Ru–Sn–B/Al_2O_3 catalysts [31]. Pouilloux et al. [15] found that the increase of the tin content of Ru–Sn–B/Al_2O_3 catalysts does not change significantly the catalyst activity for hydrogenation of methyl oleate because there are different reaction mechanisms at different tin contents. The results of the present work showed that the activity decreases with the increase of Ge content. Ge atoms presumably blocks Ru hydrogenolytic ensembles upon its deposition on the Ru aggregates. It can also be seen that the conversion after 120 min of reaction remains virtually unchanged.

The fact that full conversion was not achieved on most catalyst even at long reaction times (360 min) was unexpected. Only the Ru–B catalyst permitted a conversion of 100%, probably because Ge strongly decreases the hydrogenation activity of Ru. This is reflected by the decrease of the cyclohexane conversion from 43.2% to 4.8% in the Ru–B/Al_2O_3 to Ru–Ge(4.0)–B/Al_2O_3 catalyst series. The initial reaction rate was almost the same for all the catalysts but after 2 h reaction time the conversion reached a plateau. This behavior in a batch type reactor can be explained by the occurrence of two phenomena: (i) thermodynamic limitations or (ii) catalysts deactivation. Thermodynamic limitation can be excluded because with Ru–B catalysts a conversion of 100% was achieved. The deactivation could be due to coke deposition or metal phase sintering. The deposition a small amount of coke on the metal surface can easily deactivate the hydrogenation function of the catalyst. The elucidation of the deactivation mechanism would require more experimental work.

Percent values of reaction products yields and conversion (%) at 120 min are given in Table 3. At this reaction time methyl oleate conversion has reached its higher value for all catalysts. At higher

Table 2
Results of XPS studies performed on more representative catalysts.

Catalyst	Ru/Al bulk	Ru/Al XPS	$Ru^{\circ}/(Ru^{\circ} + Ru^{n+})$ XPS	Ge/Al bulk	Ge/Al XPS	B/Al XPS
Ru–B	0.0051	0.0038	0.48	–	–	0.009
Ru–Ge(1.0)–B	0.0052	0.0222	0.47	0.0072	0.021	0.081
Ru–Ge(4.0)–B	0.0053	0.0092	0.38	0.0296	0.081	0.088

Table 3
Percent values of conversion and yield to different products at 120 min reaction time. Ru(1%)–Ge(x)–B/Al_2O_3 catalysts.

Catalysts	Conversion (%)	Oleyl alcohol (%)	Stearyl alcohol (%)	Methyl stearate (%)
Ru–B	99.46	0.00	98.00	1.46
Ru–Ge(0.5)–B	86.00	0.00	43.14	42.86
Ru–Ge(1.0)–B	89.06	2.30	27.29	59.47
Ru–Ge(2.0)–B	78.57	19.45	8.58	50.54
Ru–Ge(4.0)–B	61.30	0.72	10.15	50.43

reaction times the oleyl alcohol is further transformed into stearyl alcohol which is the final product in the reaction scheme. It can be seen in Table 3 that monometallic catalyst is the most active, and its hydrogenating activity is enough high to hydrogenate nearly all C—C and C—O bonds. As the Ge content is increased the formation of stearyl alcohol and methyl stearate decreases. Moreover, it can be seen in Table 3 that the highest yield to oleyl alcohol was obtained with the Ru–Ge(2.0)–B catalyst. Higher amounts of Ge in the catalyst formulation (4 wt%) leads to an increase in methyl stearate formation. For catalysts with 1 and 2% Ge fatty alcohols (stearyl and oleyl alcohols from hydrocracking of carboxymethyl group) were only detected at the highest reaction times. The incorporation of Ge significantly modifies the hydro/dehydrogenating activity of Ru, as it can be seen in Table 3. Narasimhan et al. [6] found that the maximum selectivity to oleyl alcohol is obtained with an atomic ratio Ru:Sn = 2. This is because the increase in the amount of Sn favors the Sn–Ru interaction enhancing the selectivity toward oleyl alcohol [11]. The same effect can be expected when Ge is added. If the Ge content is high (4 wt%), the ability to hydrogenate the C—O group becomes low, whereas the remaining hydrogenating activity is enough to hydrogenate C—C double bonds so significant quantities of methyl stearate can be produced. As Ge content decreases, there are more Ru exposed atoms and the hydrogenating activity increases. The hydrogenation of both C—C and C—O groups may then occur leading to stearyl alcohol production.

Fig. 5 shows the yields to different reaction products and the conversion as a function of time for the catalyst with the highest selectivity (Ru–Ge(2.0)–B/Al_2O_3 catalyst). As expected the conversion continuously increases, i.e. methyl oleate concentration decreases. The yield to stearyl alcohol increases since it is a final product. Methyl stearate and oleyl alcohol show a maximum in the yield plot because they are intermediates products.

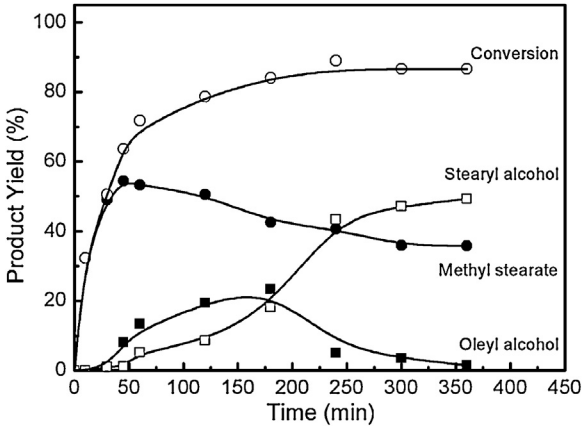

Fig. 5. Products yield and conversion as a function of time. Ru–Ge(2.0)–B/Al_2O_3 catalyst.

The highest amount of oleyl alcohol (60% selectivity) was obtained with the Ru–Ge(2.0)–B/Al_2O_3 catalyst. With Ru–Sn(2.0)–B/Al_2O_3 at the same reaction conditions an oleyl alcohol selectivity of 45% is only got [32]. Higher oleyl alcohol selectivities (70–80%) have been reported by other researchers using Ru–Sn/Al_2O_3 catalysts [14,15]. Co–Sn–B/Al_2O_3 catalysts have been also reported with an oleyl alcohol selectivity of 70% [33,34]. Ru–Sn–B/ZnO catalysts have low reported selectivity values (40%) to unsaturated alcohols [35].

4. Conclusions

The results of catalyst characterization by TPR and XPS show that Ge is deposited both on the metal function and on the support. The fraction of Ge deposited on the metal function is in strong interaction with Ru, so that its metallic activity is significantly modified. The dehydrogenation and hydrogenolysis activity of Ru are strongly diminished by Ge addition. The Ge/Ru = 2 is the optimum ratio for higher oleyl alcohol production.

References

[1] B. Miya, US Patent 4,252,689 (1981).
[2] R.D. Rieke, D.S. Thakur, B.D. Roberts, G.T. White, Journal of the American Oil Chemists' Society 74 (1997) 333–339.
[3] R.D. Rieke, D.S. Thakur, B.D. Roberts, G.T. White, Journal of the American Oil Chemists' Society 74 (1997) 341–345.
[4] U.R. Kreutze, Journal of the American Oil Chemists' Society 61 (1984) 343–348.
[5] T. Turek, D.L. Trimm, N.W. Cant, Catalysis Reviews: Science and Engineering 36 (1994) 645–683.
[6] C.S. Narasimhan, V.M. Deshpande, K. Ramnarayan, Journal of Catalysis 121 (1990) 174–182.
[7] F.T. Van de Scheur, L.H. Staal, Applied Catalysis A: General 108 (1994) 63–83.
[8] T. Miyake, T. Makino, S. Taniguchi, H. Watanuki, T. Niki, S. Shimizu, Y. Kojima, M. Sano, Applied Catalysis A: General 364 (2009) 108–112.
[9] S.A. da, S. Corradini, G.G. Lenzi, M.K. Lenzi, C.M.F. Soares, O.A.A. Santos, Journal of Non-Crystalline Solids 354 (2008) 4865–4870.
[10] C.S. Narasimhan, V.M. Deshpande, K. Ramnarayan, Applied Catalysis A: General 48 (1989) L1–L6.
[11] M.A. Sánchez, V.A. Mazzieri, M.R. Sad, R. Grau, C.L. Pieck, Journal of Chemical Technology and Biotechnology 86 (2011) 447–453.
[12] D.S. Brands, E.K. Poels, T.A. Krieger, O.V. Makarva, C. Weber, S. Veer, A. Bliek, Catalysis Letters 36 (1996) 175–181.
[13] T. Fleckenstein, J. Pohl, F.J. Carduck, US Patent 5,043,485 (1991).
[14] D.A. Echeverri, J.M. Marín, G.M. Restrepo, L.A. Rios, Applied Catalysis A: General 366 (2009) 342–347.
[15] Y. Pouilloux, F. Autin, C. Guimon, J.J. Barrault, Journal of Catalysis 176 (1998) 215–224.
[16] P. Gallezot, D. Richard, Catalysis Reviews. Science and Engineering 40 (1998) 81–126.
[17] V.A. Mazzieri, J.M. Grau, J.C. Yori, C.R. Vera, C.L. Pieck, Applied Catalysis A: General 354 (2009) 161–168.
[18] T. Ekou, A. Flura, L. Ekou, C. Especel, S. Royer, Journal of Molecular Catalysis A: Chemical 353/354 (2012) 148–155.
[19] M.C. Schoenmaker-Stolk, J.W. Verwijs, J.J.F. Scholten, Applied Catalysis A: General 30 (1987) 339–352.
[20] S.R. de Miguel, O.A. Scelza, A.A. Castro, Applied Catalysis 44 (1988) 23–32.
[21] M.J. Mendes, O.A.A. Santos, E. Jordão, A.M. Silva, Applied Catalysis A: General 217 (2001) 253–262.
[22] K.-Y. Cheah, T.S. Tang, F. Mizukami, S. Niwa, M. Toba, Y.M. Choo, Journal of the American Oil Chemists' Society 69 (1992) 410–416.
[23] L. Jinxiang, Y. Lixin, G. Shiuying, H. Licuan, T. Renyuan, L. Dongbai, Thermochimica Acta 123 (1988) 121–133.

[24] S.H. Xie, M.H. Qiao, H.X. Li, W.J. Wang, J.F. Deng, Applied Catalysis A: General 176 (1999) 129–134.
[25] J.F. Moulder, W.F. Stickle, P.E. Sobol, Handbook of X-ray Photoelectron Spectroscopy, Perkin-Elmer Corporation, Eden Prairie, Minnesota, 1992.
[26] C. Elmasides, D.I. Kondarides, W. Grünert, X.E. Verykios, The Journal of Physical Chemistry B 103 (1999) 5227–5239.
[27] V.A. Mazzieri, F. Coloma-Pascual, A. Arcoya, P.C. L'Argentière, N.S. Fígoli, Applied Surface Science 210 (2003) 222–230.
[28] Y. Okamoto, Y. Nitta, T. Imanaka, S. Teranishi, Journal of the Chemical Society, Faraday Transactions 75 (1979) 2027–2039.
[29] C.D. Wagner, W.M. Riggs, L.E. Davis, J.F. Moulder, G.E. Muilenberg, Handbook of X-ray Photoelectron Spectroscopy, Perkin-Elmer Co., Eden Prairie, Minnesota, 1979 (Physical Electronics) 88–89.
[30] A. Borgna, T.F. Garetto, C.R. Apesteguia, B. Maroweck, Applied Catalysis A: General 182 (1999) 189–197.
[31] V.A. Mazzieri, M.R. Sad, C.R. Vera, C.L. Pieck, R. Grau, Química Nova 33 (2010) 269–272.
[32] M.A. Sánchez, V.A. Mazzieri, M.R. Sad, C.L. Pieck, Reaction Kinetics Mechanisms and Catalysis 107 (2012) 127–139.
[33] Y. Pouilloux, F. Autin, A. Piccirilli, C. Guimon, J. Barrault, Applied Catalysis A: General 169 (1998) 65–75.
[34] Y. Pouilloux, F. Autin, J. Barrault, Catalysis Today 63 (2000) 87–100.
[35] K. De Oliveira, Y. Pouilloux, J. Barrault, Journal of Catalysis 204 (2001) 230–237.